CASE 1: SIMULATION OF A SYNTHETIC JET IN QUIESCENT AIR USING TLNS3D FLOW CODE

Veer N. Vatsa[1] and Eli Turkel[2]

[1] *Computational Modeling & Simulation Branch, NASA Langley Research Center, Hampton, VA*
[2] *Tel Aviv University, Israel & NIA, Hampton, VA*

Governing Equations and Solution Methodology

In the present work, a generalized form of the thin-layer Navier-Stokes equations is used to model the turbulent, viscous flow encountered in a synthetic jet. The equation set is obtained from the complete Navier-Stokes equations by retaining the viscous diffusion terms normal to the solid surfaces in every coordinate direction. For a body-fitted coordinate system (ξ, η, ζ) fixed in time, these equations can be written in the conservative form as:

$$J\frac{\partial(\mathbf{U})}{\partial t} \quad + \quad \frac{\partial(\mathbf{F}-\mathbf{F_v})}{\partial \xi} + \frac{\partial(\mathbf{G}-\mathbf{G_v})}{\partial \eta} + \frac{\partial(\mathbf{H}-\mathbf{H_v})}{\partial \zeta} \;=\; 0 \tag{1}$$

where $\mathbf{U}$ represents the conserved variable vector. The vectors $\mathbf{F}$, $\mathbf{G}$, $\mathbf{H}$, and $\mathbf{F_v}$, $\mathbf{G_v}$, $\mathbf{H_v}$ represent the convective and diffusive fluxes in the three transformed coordinate directions, respectively. In Eqn. (1), J represents the cell-volume or the Jacobian of coordinate transformation. A multigrid based, general purpose multi-block structured grid approach is used for the solution of the governing equations. In particular, the TLNS3D flow code is used in this study to solve Eqn. (1). Several references exist describing the discretization and algorithmic details of TLNS3D code. We include only a brief summary of the general features, and refer to the work of Vatsa and co-workers [1, 2] for further details regarding the TLNS3D code.

Numerical Discretization

The spatial terms in Eqn. (1) are discretized using a standard cell-centered finite-volume scheme. The convection terms are discretized using second-order central differences with scalar/matrix artificial dissipation (second- and fourth- difference dissipation) added to suppress the odd-even decoupling and oscillations in the vicinity of shock waves and stagnation points [3, 4]. The viscous terms are discretized with second-order accurate central difference formulas [1]. For the present computations, the Spalart-Allmaras (SA) model [5] and the Menter's SST model [6] are used for simulating turbulent flows.

For temporal discretization, the convective and diffusive terms are grouped together, and Eqn. (1) can be rewritten as:

$$\frac{d\mathbf{U}}{dt} = -C(\mathbf{U}) + D_p(\mathbf{U}) + D_a(\mathbf{U}) \tag{2}$$

where $C(\mathbf{U})$, $D_p(\mathbf{U})$, and $D_a(\mathbf{U})$ are the convection, physical diffusion, and artificial diffusion terms, respectively. The cell-volume or the Jacobian of coordinate transformation being included in these terms. The time-derivative term can be approximated to any desired order of accuracy by the Taylor series

$$\frac{d\mathbf{U}}{dt} = \frac{1}{\Delta t}[a_0\mathbf{U}^{n+1} + a_1\mathbf{U}^n + a_2\mathbf{U}^{n-1} + a_3\mathbf{U}^{n-2} + ...] \tag{3}$$

Eqn. (3) represents a generalized backward difference scheme (BDF) in time, where the order of accuracy is determined by the choice of coefficients a_0, a_1, a_2 ... etc. For example, if $a_0 = 1.5$, $a_1 = -2$ and $a_2 = .5$, it results in a second-order accurate scheme (BDF2) in time, which is the primary scheme chosen for this work due to its robustness and stability properties [7].

In Eqn. (3), the superscript n represents the time level at which the solution is known, and n+1 refers to the next time level to which the solution will be advanced. Similarly, n-1 refers to the solution at one time level before the current solution. Regrouping the time-dependent terms and the original steady-state operator leads to the equation:

$$\frac{a_0}{\Delta t}\mathbf{U}^{n+1} + \frac{E(\mathbf{U}^{n,n-1,..})}{\Delta t} = S(\mathbf{U}^n) \tag{4}$$

where $E(\mathbf{U}^{n,n-1,..})$ depends only at solution vector at time levels n and prior, and S represents the steady state operator or the right hand side of Eqn.(2). By adding a pseudo-time term, we can rewrite the above equation as:

$$\frac{\partial \mathbf{U}}{\partial \tau} + \frac{a_0}{\Delta t}\mathbf{U}^{n+1} + \frac{E(\mathbf{U}^{n,n-1,..})}{\Delta t} = S(\mathbf{U}^n) \tag{5}$$

Solution Algorithm

The algorithm used here for solving unsteady flows relies heavily on the steady-state algorithm available in the TLNS3D code [1]. The basic algorithm consists of a five-stage Runge-Kutta time-stepping scheme for advancing the solution in pseudo-time, until the solution converges to a steady-state. Efficiency of this algorithm is enhanced through the use of local time-stepping, residual smoothing and multigrid techniques developed for solving steady-state equations. In order to solve the time-dependent Navier-Stokes equations (Eqn. 5), we added another iteration loop in physical time outside the pseudo-time iteration loop in TLNS3D. For fixed values of $S(\mathbf{U}^n)$, $E(\mathbf{U}^{n,n-1,..})$, we iterate on $\mathbf{U}^{n+1}$ using the standard multigrid procedure of TLNS3D developed for steady-state, until desired level of convergence is achieved. This strategy, originally proposed by Jameson [8] for Euler equations and adapted for the TLNS3D viscous flow solver by Melson et. al [7] is popularly known as the dual time-stepping scheme for solving unsteady flows. The process is repeated until the desired number of time-steps have been completed. The details of the TLNS3D flow code for solving unsteady flows are available in Refs. [7] and [9].

Boundary Conditions

Except for the moving diaphragm, standard boundary conditions, such as the no-slip, no injection, fixed wall temperature or adiabatic wall, far-field and extrapolation conditions are used as appropriate for the various boundaries. The most accurate procedure to simulate the moving diaphragm would require moving grid capability. For simplicity, we chose to simulate this type of boundary condition by a periodic transpiration velocity condition. The frequency of the transpiration velocity at the diaphragm surface in the numerical simulation corresponded to the frequency of the oscillating diaphragm, and the peak velocity at the diaphragm surface was obtained from numerical iteration so as to match the experimentally measured peak velocity of the synthetic jet emanating from the slot exit. The pressure at the moving diaphragm is also required for closure. However, in the absence of unsteady pressure data from the experiment, we imposed a zero pressure gradient at the diaphragm boundary. We also tested the pressure gradient boundary condition obtained from one-dimensional normal momentum equation [10], which had very little impact on the solutions. Due to the simplicity and robustness, we selected the zero pressure gradient boundary condition at the diaphragm surface.

Implementation and Case Specific Details

Although the actuator geometry is highly three-dimensional, the outer flow field is nominally two-dimensional because of the high aspect ratio of the rectangular slot. For the present study, this configuration is modeled as a two-dimensional problem. A multi-block structured grid available at the CFDVAL2004 website is used as a baseline grid.

The periodic motion of the diaphragm is simulated by specifying a sinusoidal velocity at the diaphragm surface with a frequency of 450 Hz., corresponding to the experimental setup. The amplitude is chosen so that the maximum Mach number at the jet exit is approximately 0.1, to replicate the experimental conditions. At the solid walls zero slip, zero injection, adiabatic temperature and zero pressure gradient conditions are imposed. In the external region, symmetry conditions are imposed on the side (vertical) boundaries and far-field conditions are imposed on the top boundary. A nominal free-stream Mach number of 0.001 is imposed in the free stream to simulate incompressible flow conditions in the TLNS3D code, which solves compressible flow equations.

The code was run in unsteady (URANS) mode until the periodicity was established. The time-mean quantities were obtained by running the code for at least another 15 periods and averaging the flow quantities over these periods. The phase-locked average of flow quantities were assumed to be coincident with their values during the last full time period.

Results/Discussion

Only a brief set of results is included here, detailed results will be available in the workshop proceedings. Majority of the solutions were obtained with SA turbulence model on the baseline grid with a time-step of $\Delta t = T_{period}/72$, where T_{period} represents the physical time for a complete period. In addition, results were generated for the following conditions: (a) coarser grid (cg) obtained by eliminating every other point from the baseline grid; (b) finer grid (fg) generated by increasing resolution in the normal direction by 50%; (c) lower time-step (lower dt), where $\Delta t = T_{period}/144$; and (d) Menter's SST turbulence model. The results for the vertical velocity near the slot exit center line (x=0., y=0.1 mm) from these computations are compared in Fig. 1, which shows very little sensitivity to turbulence model change, and spatial and temporal resolutions.

Next we show the results for time-averaged velocity along the jet center line in Fig. 2. In the proximity of the slot exit (y $<$ 2 mm), all 5 sets of results are indistinguishable, and are in good agreement with the hotwire data. However, further away from the slot, the coarse grid (cg) results show significant deviation from the baseline results. The effect of turbulence model type (SA or SST) are also more pronounced in the outer region. Similar trends are observed in Fig. 3 for the jet width based on time-averaged solutions.

Based on these results and more detailed comparisons (not shown here) of the computational results for time-averaged and phase-locked average velocities, the effect of lowering the time-step and refining the normal mesh were found to be very small. Noticeable differences were observed for the coarse grid (cg) results in the outer regions. The difference between the SA and SST turbulence model results become more pronounced in regions further away from the slot exit.

References

[1] Vatsa, V.N. and Wedan, B.W.: "Development of a multigrid code for 3-d Navier-Stokes equations and its application to a grid-refinement study". Computers and Fluids. 18:391-403. 1990.

[2] Vatsa, V.N.; Sanetrik, M.D.; and Parlette, E.B.: "Development of a Flexible and Efficient Multigrid-Based Multiblock Flow Solver". AIAA paper 93-0677, Jan. 1993.

[3] Turkel, E. and Vatsa, V.N.: "Effect of artificial viscosity on three-dimensional flow solutions". AIAA Journal, vol. 32, no. 1, Jan. 1994, pp. 39-45.

[4] Jameson, A.; Schmidt, W.; and Turkel, E.: "Numerical Solutions of the Euler Equations by Finite Volume Methods Using Runge-Kutta Time-Stepping Schemes". AIAA Paper 1981-1259, June 1981.

[5] Spalart, P.A. and Allmaras, S.R.:"A one-equation turbulence model for aerodynamic flows". AIAA Paper 92-439, Reno, NV, Jan. 1992.

[6] Menter, F.R.: "Zonal Two Equation k-ω Turbulence Models for Aerodynamic Flows". AIAA paper 93-2906, Orlando, Fl, 1993.

[7] Melson,N.D.; Sanetrik, M.D.; and Atkins, H.L.:"Time-accurate calculations with multigrid acceleration". Appeared in "Proceedings of the Sixth Copper Mountain conference on multigrid methods", 1993, edited by: Melson, N.D.; Manteuffel, T.A.; and S.F. McCormick, S.F.

[8] Jameson, A.: "Time Dependent Calculations Using Multigrid, with Applications to Unsteady Flows past Airfoils and Wings". AIAA Paper 91-1596, 1991.

[9] Bijl, H.; Carpenter, M.H.; and Vatsa, V.N.: "Time Integration Schemes for the Unsteady Navier-Stokes Equations". AIAA Paper 2001-2612.

[10] Rizzetta, D.P.; Visbal. M.R.; and Stanek, M.J.: "Numerical Investigation of Synthetic Jet Flowfields". AIAA Paper 98-2910, June 1998.

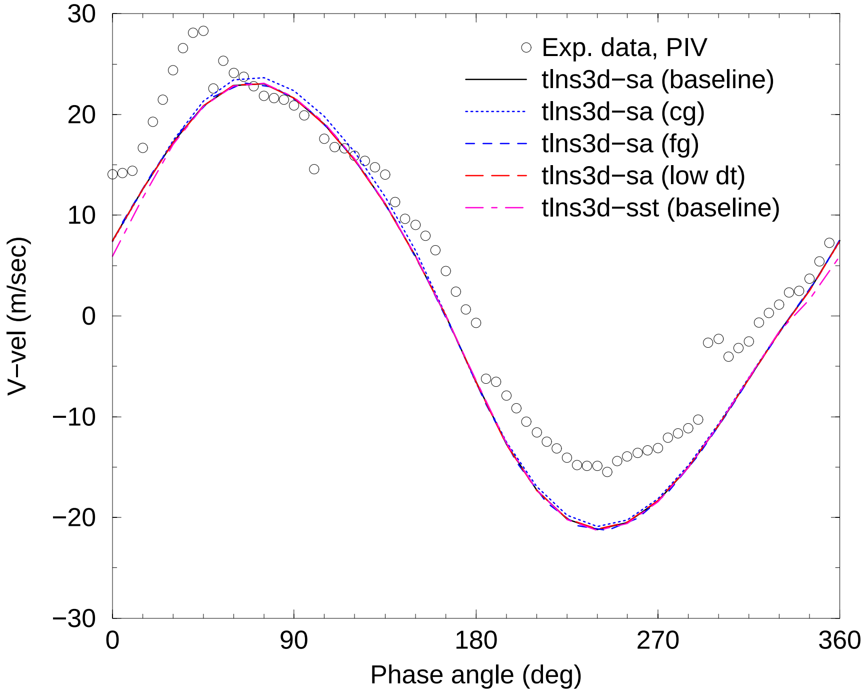

Figure 1: Time-variation of V-velocity at slot exit, x=0., y=0.1 mm

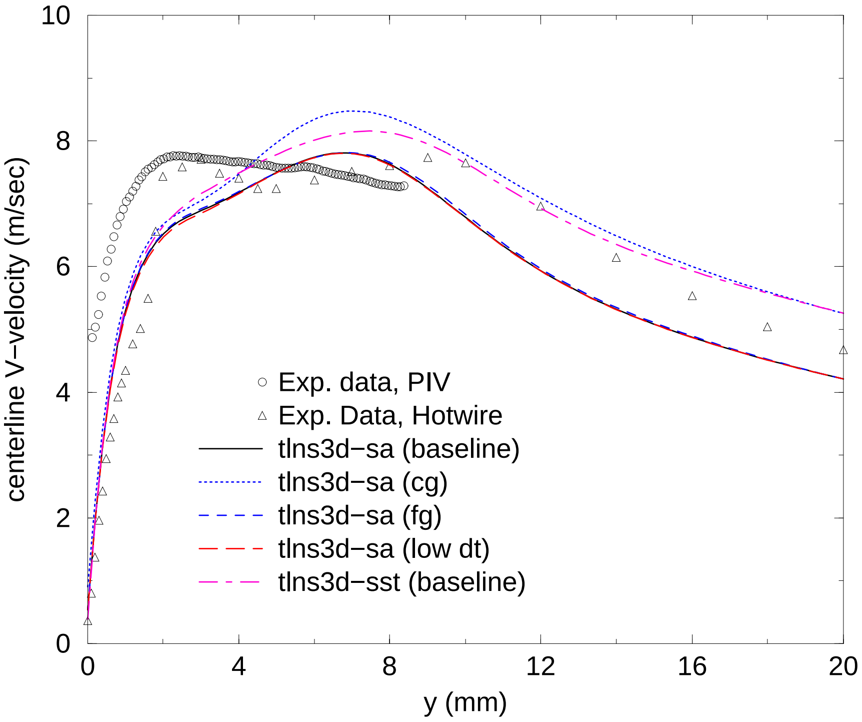

Figure 2: Center-line average velocity comparisons

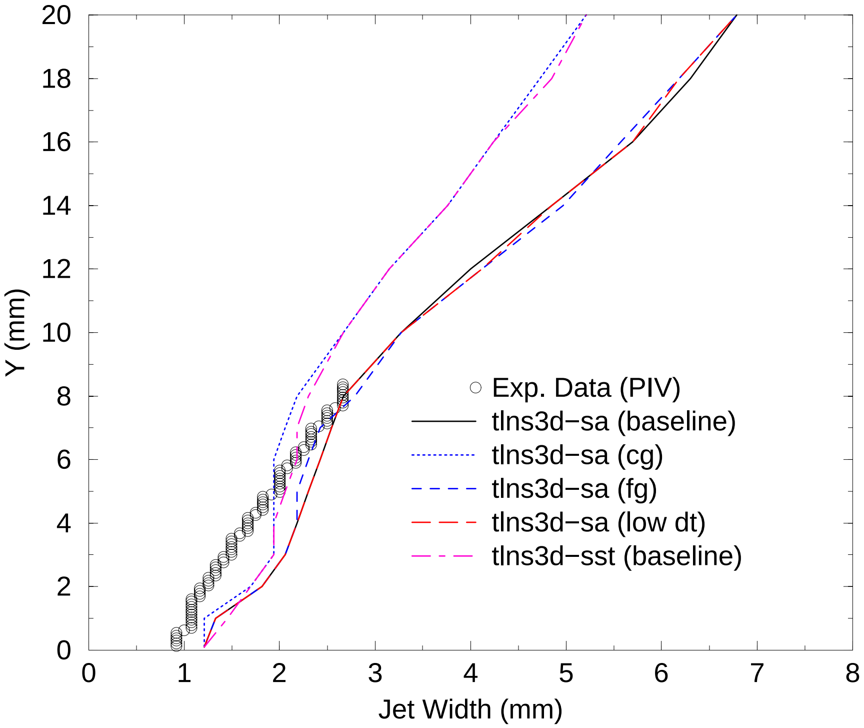

Figure 3: Jet-width comparisons